The Japan Society
of Applied Physics

REGULAR PAPER

Analysis of an I/O metal grating coupler for organic membrane photonic integrated circuits

View the article online for updates and enhancements.

REGULAR PAPER

Analysis of an I/O metal grating coupler for organic membrane photonic integrated circuits

Keisuke Masuda[1*], Tomohiro Amemiya[1,2], Hibiki Kagami[2], Makoto Tanaka[1], Nobuhiko Nishiyama[1,2], and Shigehisa Arai[1,2]

[1]Department of Electrical and Electronic Engineering, Tokyo Institute of Technology 2-12-1-S9-7 O-okayama, Meguro-ku, Tokyo, 152-8550, Japan
[2]Institute of Innovative Research (IIR), Tokyo Institute of Technology 2-12-1-S9-7 O-okayama, Meguro-ku, Tokyo, 152-8552, Japan

*E-mail: masuda.k.ap@m.titech.ac.jp

We propose organic membrane photonic integrated circuits (OMPICs), which can collectively integrate various optical elements into a thin film and can realize wearable devices and high-speed optical signal processing by making more flexible photonic integrated circuits. In OMPICs, vertical grating couplers are effective as input and output ports. In this study, we propose three types of structure: an SU-8/Cytop grating coupler, a metal grating coupler, and a modified metal grating coupler with a metal mirror and an SU-8/Cytop distributed Bragg reflector. We analyze the optical coupling efficiency in each case. © 2019 The Japan Society of Applied Physics

1. Introduction

In recent years, mechanically flexible optical systems have been finding applications in short-range data communication,[1–3] various sensors,[4–7] wearable devices for health care,[8–12] etc. These optical systems make the best use of the low-loss property and flexibility of organic materials; many research groups have published various reports including the development of the roll-to-roll manufacturing process.[13–16] However, compared with standard optical devices based on conventional rigid platforms (III-V semiconductors and Si),[17–21] most reports so far on organic material-based optical devices show a single function in one chip.[22,23] Therefore, organic material-based optical devices are still far from their inorganic counterparts in terms of integration and functionality.

Against this backdrop, we have proposed organic membrane photonic integrated circuits (OMPICs),[24] which can incorporate the various functions needed for an optical system into a flexible organic membrane (see Fig. 1). In flexible OMPICs, lateral I/O coupling (i.e., input/output from a cleaved edge of a waveguide) is not easy because of the difficulty of position matching, in addition to the mode size mismatch between its fiber and the waveguide. Therefore, here we propose three types of vertical grating couplers, which are suitable for OMPICs: an SU-8/Cytop grating coupler, a metal grating coupler, and an improved metal grating coupler with a metal mirror and an SU-8/Cytop distributed Bragg reflector. In the following sections, after simulating the characteristics of a waveguide for OMPICs, we analyze the optical coupling efficiency in each case.

2. Analysis of the waveguide for OMPICs

2.1. Design of the waveguide structure

Before analyzing the vertical grating couplers for OMPICs, we first calculated the characteristic parameters of a waveguide that is monolithically integrated in an organic membrane. Figure 2(a) shows the structure of a waveguide along the cross-section perpendicular to the direction of light propagation. We adopted SU-8[25] (refractive index 1.59 at a wavelength of 1550 nm) as the core material and Cytop[26] (refractive index 1.34 at a wavelength of 1550 nm) as the cladding material. Other physical properties except refractive
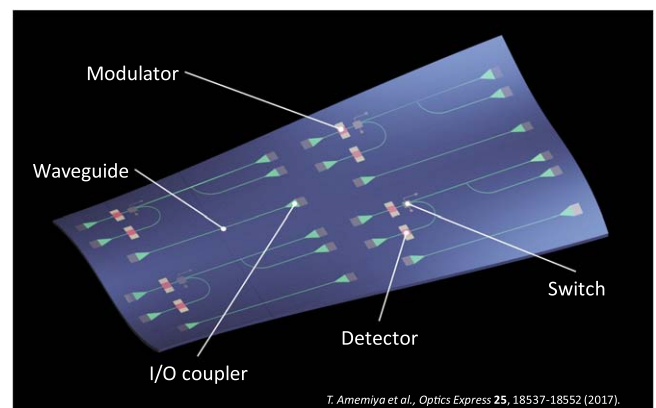
Fig. 1. (Color online) Conceptual diagram of an organic membrane photonic integrated circuit.
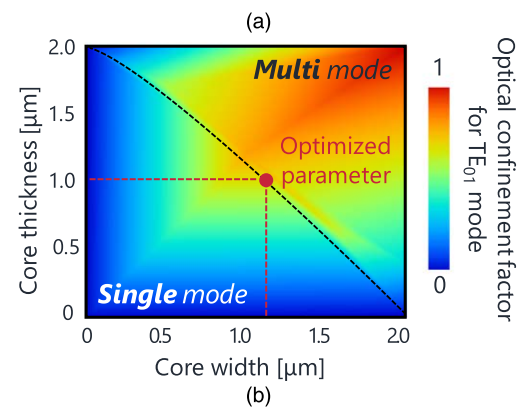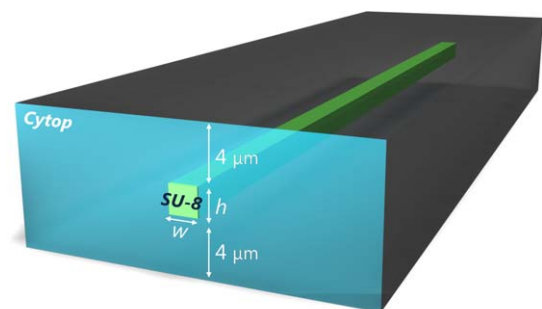
Fig. 2. (Color online) (a) Bird's eye view of the waveguide; (b) confinement factor of the TE_0 mode as a function of SU-8 core width and thickness.
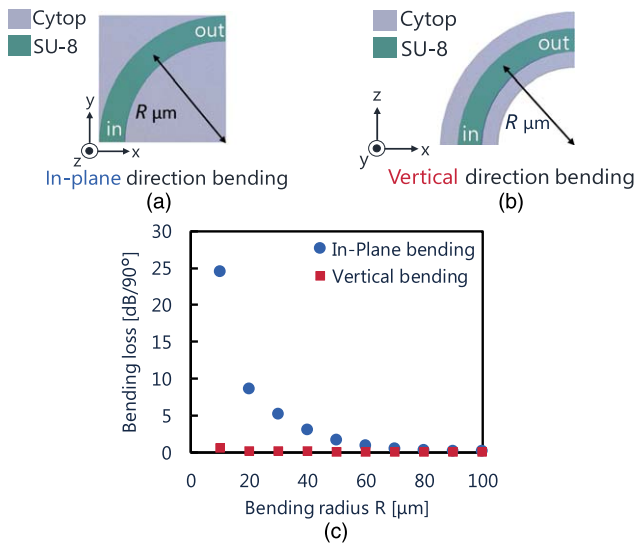
Fig. 3. (Color online) (a) Schematic image of in-plane bending. (b) Schematic image of vertical direction bending. (c) Calculated in-plane and vertical bending loss at 90° bending as a function bending radius *R*.

index can be found in Refs. 25 and 26. In the calculation, the upper and lower cladding thicknesses were fixed at 4 μm; the width w and thickness h of the core layer were set as parameters. We simulated the propagation of light in the waveguide, using the finite-element method, at a wavelength of 1550 nm. Figure 2(b) shows the result of plotting the confinement factor of the TE_0 mode. The black dotted line is the limit at which single-mode propagation can be maintained; the left and right sides of the black dotted line are the single-mode and multi-mode operation regions, respectively. In order to reduce propagation loss and bending loss of the waveguide in OMPICs, the confinement factor should be as high as possible while maintaining single-mode propagation. As a result, w and h were set to 1.2 μm and 1.0 μm. Here, the values of w and h are different because the shape of the waveguide is asymmetric in the vertical and horizontal directions (i.e., unlike in the horizontal direction, the SU-8 core is sandwiched by air in the vertical direction).

2.2. Bending loss of the waveguide
Next, we simulated the bending loss of the waveguide using the finite-difference time-domain (FDTD) method. In the case of OMPICs, in addition to in-plane bending loss [i.e., bending inside optical circuits as shown in Fig. 3(a)], we also need to simulate vertical bending loss [i.e., physical bending of the film as shown in Fig. 3(b)].

Figure 3(c) shows the calculated in-plane and vertical bending loss at 90° bending as a function of the bending radius (blue and red plots show results for in-plane and vertical bending, respectively). As observed, the in-plane bending loss is 0.5 dB or lower for a bend radius of 70 μm while the vertical bending loss is lower than 0.5 dB for a bend radius of 20 μm. Figure 3(c) reveals that the vertical bending loss tends to be smaller than the in-plane bending loss. This is because the SU-8 core is sandwiched by air, which has a low refractive index, through the Cytop cladding (i.e., a high refractive index contrast around the core is realized). For a bend radius of 20 μm, the ratio of the optical intensity
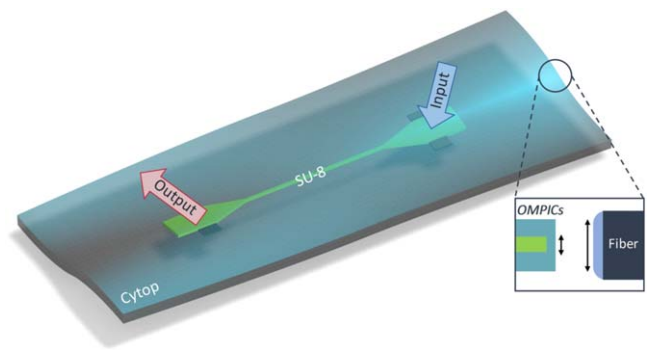
Fig. 4. (Color online) Waveguide and vertical grating coupler monolithically integrated on an organic membrane.

distribution leaking into the air is about 15% at the maximum.

3. Analysis of the I/O vertical grating coupler for OMPICs

3.1. Device structure
In OMPICs, from the viewpoint of their thinness and its flexibility, it is difficult to send an input signal and extract an output signal from the end faces of the waveguide as in ordinary optical circuits. Therefore, it is effective to inject light from the vertical direction using a grating coupler[27] as shown in Fig. 4.

In general, it is difficult to obtain a sufficient refractive index contrast necessary for a grating coupler (i.e., relatively high coupling coefficient) in an organic material platform. Therefore, we adopted vertical coupling using a buried metal grating. The grating coupler is assumed to be connected to the waveguide through a tapered waveguide to realize single-mode propagation (see the structure given in Fig. 4). In this study, the width and length of the taper were fixed to 15 μm and 100 μm, respectively.

3.2. Analysis of coupling efficiency in each grating coupler
Figures 5(a) and 5(b) depict an organic material-based grating coupler composed of SU-8 and Cytop and a metal grating coupler with thin gold stripes buried in the SU-8 core of the waveguide, respectively. Using the FDTD method, we first simulated the propagation of light to calculate the coupling efficiencies for these two grating couplers. The grating thickness h [SU-8 thickness in Fig. 5(a), metal thickness in Fig. 5(b)] and the grating period Λ were set as parameters. In this analysis, the wavelength and angle of the TE-mode input light were fixed at 1550 nm and 92°. In addition, the duty ratio (i.e., The ratio of the metal region to the grating period Λ for the metal grating, and the ratio of the SU-8 region to the grating period Λ for the SU-8/Cytop grating) was fixed at 50%.

Figure 6 shows calculated coupling efficiencies as a function of the grating period Λ, with the grating thickness h as a parameter. The figure shows that for the SU-8/Cytop grating coupler, the coupling efficiency reaches a maximum of -12.2 dB with Λ of 1.18 μm and h of 0.6 μm. For the metal grating, the coupling efficiency reaches a maximum of -5.8 dB with Λ of 1.1 μm and h of 0.12 μm. Compared with
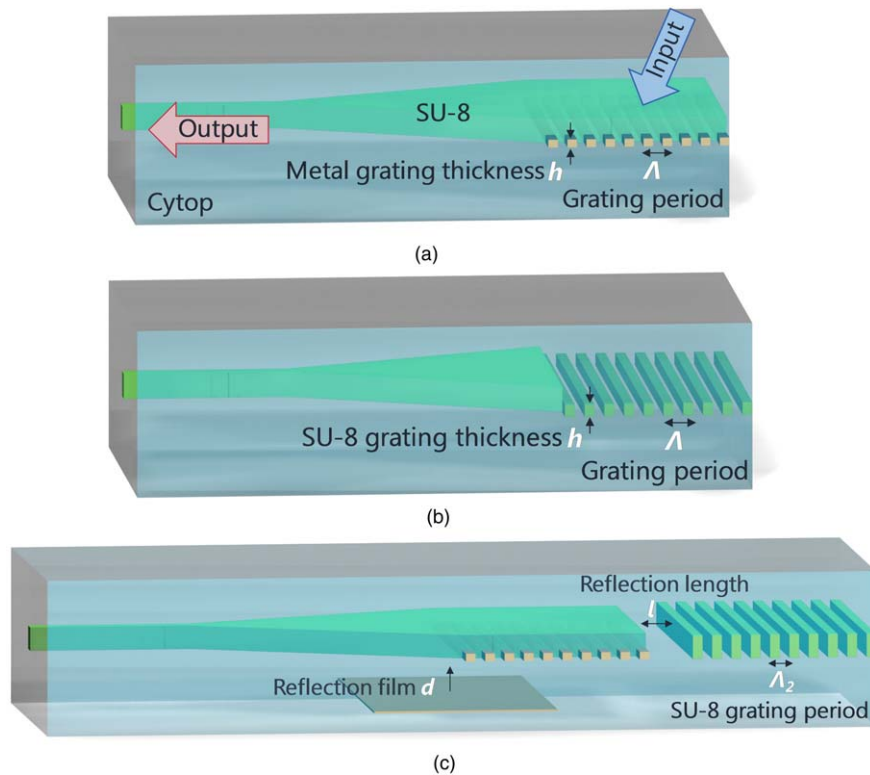
Fig. 5. (Color online) Three kinds of grating couplers for OMPICs used in the simulation. (a) SU-8/Cytop grating coupler. (b) Metal grating coupler. (c) Improved metal grating coupler with a gold mirror and an SU-8/Cytop distributed Bragg reflector (DBR).
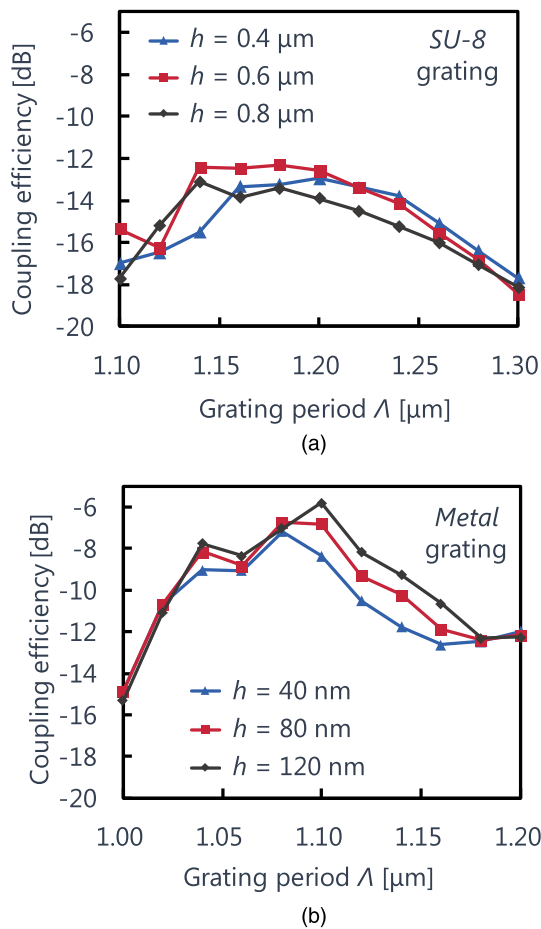
Fig. 6. (Color online) Calculated coupling efficiencies as a function of the grating period, with the grating thickness as a parameter. (a) SU-8/Cytop grating coupler. (b) Metal grating coupler.

the SU-8/Cytop grating coupler, it is suggested that an even higher coupling coefficient can be realized by embedding gold stripes inside the core. Figure 8(a) visualizes one example of the optical field distribution for the metal grating coupler, showing how light incident on the grating propagates to the waveguide. Further improvement is, however, required for this structure because downward and backward radiation cannot be ignored (especially downward). Therefore, we considered a metal grating coupler added with a gold mirror[28,29] inside the lower cladding layer and an SU-8/Cytop DBR at the back of the grating [see Fig. 5(c)].

In order to confirm the contribution of the gold mirror to device performance, we first calculated the coupling efficiency of the metal grating coupler with the gold mirror inside the lower cladding layer. In the simulation process, the thickness of the gold mirror was set to 5 nm, and the distance d from the grating to the gold mirror was set as a parameter. The coupling efficiency as a function of d is shown in Fig. 7(a), where the grating period Λ, grating thickness h, and number of the gratings are fixed at 1.1 μm, 120 nm, and 30, respectively. The coupling efficiency shows periodic changes associated with phase matching and takes peak values at d of 2.7 μm.

After optimizing the distance from the grating to the gold mirror, we next investigated the contribution of the SU-8/Cytop DBR at the back of the grating. Figure 7(b) shows the coupling efficiency of the device shown in Fig. 5(c) as a function of distance l from the grating to the DBR (the grating period and number of the DBR were fixed at 1.65 μm and 30, respectively, so as to obtain maximum reflectance). The coupling efficiency shows periodic changes associated with phase matching and takes peak values of -1.8 dB at $l = 0.6$ μm.
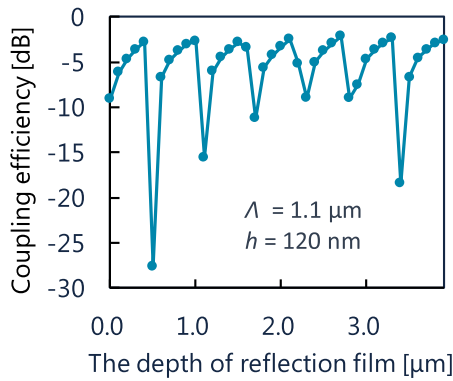
(a)
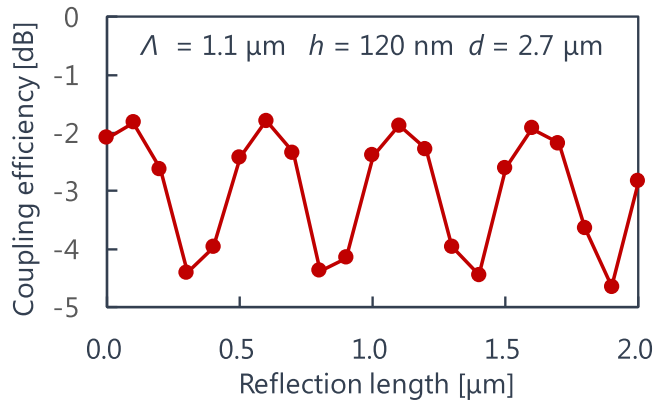
(b)

Fig. 7. (Color online) (a) Calculated coupling efficiencies as a function of the distance from the grating to the gold mirror. (b) Calculated coupling efficiencies as a function of the distance from the grating to the SU-8/Cytop DBR.

Figure 8(b) visualizes the optical field distribution for the optimized device. This result shows that the gold mirror and the SU-8/Cytop DBR function extremely well to improve the coupling efficiency.

3.3. Wavelength dependence of each grating coupler
Finally, we simulated the wavelength dependence of the coupling efficiency using the structural parameter obtained in Sect. 3.2 which gives the maximum coupling efficiency at
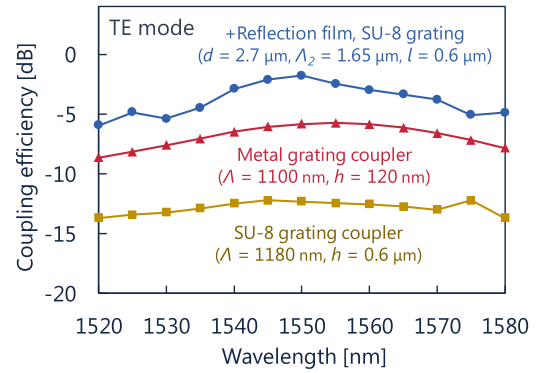
Fig. 9. (Color online) Coupling efficiencies as a function of wavelength for each kind of grating coupler.

1550 nm. Figure 9 shows the analysis result. As a result, we found coupling fluctuations of 1.4 dB, 4.3 dB, and 4.2 dB in the SU-8/Cytop grating coupler, the metal grating coupler, and the improved metal grating coupler with the gold mirror and the DBR, respectively. Since the metal grating has a high refractive index coupling coefficient, the optical coupling efficiency is high, but it is suggested that the wavelength dependence is also large accordingly. On the other hand, we confirmed that the wavelength dependence is also large.

4. Summary
We simulated the SU-8/Cytop-based waveguide and I/O vertical grating coupler, which are the most basic elements for OMPICs. The results are summarized in Table I.

For the waveguide to obtain single-mode propagation, the width and thickness of the SU-8 core were set to 1.2 μm and 1 μm, respectively. Under these conditions, in-plane and vertical bending losses were calculated and found to be 0.5 dB or lower for a 70 μm bend radius and a 20 μm bend radius, respectively.

For the I/O coupler, we investigated three kinds of vertical grating couplers: an SU-8/Cytop grating coupler, a metal grating coupler, and an improved metal grating coupler with gold mirror and SU-8/Cytop DBR. The coupling efficiency reached a maximum of −1.8 dB for the improved metal

(a)

(b)
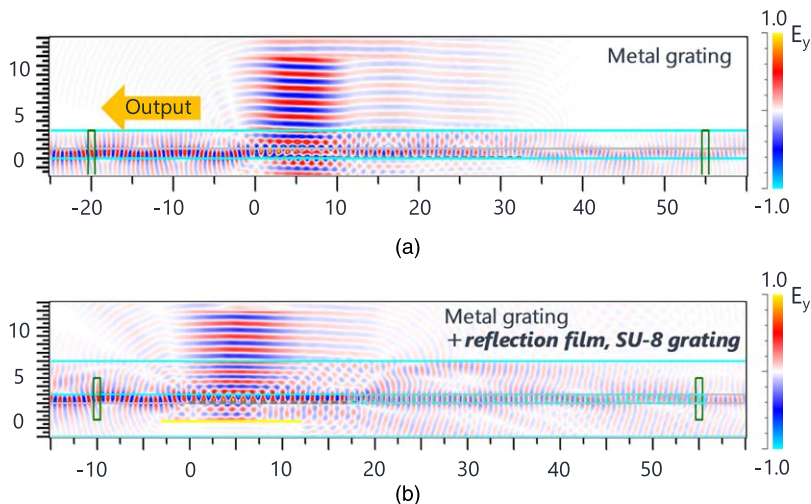
Fig. 8. (Color online) Optical field distribution, cross section of light propagation direction. (a) Metal grating coupler. (b) Improved metal grating coupler with a gold mirror and an SU-8/Cytop DBR.

Table I. Performance limit of vertical grating coupler for OMPICs, calculated for 1550 nm wavelength.

	Waveguide	I/O coupler		
		SU-8 grating	Metal grating	Metal grating + reflection film, SU-8 grating
Core material	SU-8	SU-8	SU-8	SU-8
Clad material	Cytop	Cytop	Cytop	Cytop
Calculated characteristics for TE-mode	<0.5 dB/bend ($R > 70$ μm)	-12.2 dB @$\Lambda = 1180$ nm, $h = 0.6$ μm	-5.8 dB @$\Lambda = 1100$ nm, $h = 120$ nm	-1.8 dB @$d = 2.7$ μm, $\Lambda_2 = 1.65$ μm, $l = 0.6$ μm

grating coupler with Λ of 1.1 μm and h of 120 nm, d of 2.7 μm, and l of 1 μm.

1) L. Cheng, B. E. Henty, D. D. Stancil, F. Bai, and P. Mudalige, IEEE J. Sel. Areas Commun. **25**, 1501 (2007).
2) R. Dangel, F. Horst, D. Jubin, N. Meier, J. Weiss, B. J. Offrein, B. W. Swatowski, C. M. Amb, D. J. DeShazer, and W. K. Weidner, IEEE J. Lightwave Technol. **31**, 3915 (2013).
3) L. Li, Y. Zou, H. Lin, J. Hu, X. Sun, N.-N. Feng, S. Danto, K. Richardson, T. Gu, and M. Haney, IEEE J. Lightwave Technol. **31**, 4080 (2013).
4) E. Jovanov, A. Milenkovic, C. Otto, and P. C. de Groen, J. NeuroEng. Rehabil. **2**, 6 (2005).
5) L. Fan, L. T. Varghese, Y. Xuan, J. Wang, B. Niu, and M. Qi, Opt. Express **20**, 20564 (2012).
6) S. Yun, S. Park, B. Park, Y. Kim, S. K. Park, S. Nam, and K. U. Kyung, Adv. Mater. **26**, 4474 (2014).
7) P. Yu, T. He, T. Luqi, L. Yuxing, W. Xuefeng, D. Ningqin, Y. Yi, and R. Tian-Ling, Appl. Mater. Interfaces. **8**, 26458 (2016).
8) R. S. H. Istepanian, E. Jovanov, and Y. T. Zhang, IEEE T. Inf. Technol. Biomed. **8**, 4 (2004).
9) Y.-L. Zheng, X.-R. Ding, C. C. Y. Poon, B. P. L. Lo, H. Zhang, X.-L. Zhou, G.-Z. Yang, N. Zhao, and Y.-T. Zhang, IEEE Trans. Biomed. Eng. **61**, 1538 (2014).
10) T. Yokota, P. Zalar, M. Kaltenbrunner, H. Jinno, N. Matsuhisa, H. Kitanosako, Y. Tachibana, W. Yukita, M. Koizumi, and T. Someya, Sci. Adv. **2**, e1501856 (2016).
11) J. Kim, G. A. Salvatore, H. Araki, A. M. Chiarelli, Z. Xie, A. Banks, X. Sheng, Y. Liu, J. W. Lee, and K.-I. Jang, Sci. Adv. **2**, e1600418 (2016).
12) K. Xu, Y. Lu, and K. Takei, Adv. Mater. Technol. **4**, 1800628 (2019).
13) R. Bruck, P. Muellner, N. Kataeva, A. Koeck, S. Trassl, V. Rinnerbauer, K. Schmidegg, and R. Hainberger, Appl. Opt. **52**, 4510 (2013).
14) S. Aikio, J. Hiltunen, J. Hiitola-Keinänen, M. Hiltunen, V. Kontturi, S. Siitonen, J. Puustinen, and P. Karioja, Opt. Express **24**, 2527 (2016).
15) S. Aikio, M. Zeilinger, J. Hiltunen, L. Hakalahti, J. Hiitola-Keinänen, M. Hiltunen, V. Kontturi, S. Siitonen, J. Puustinen, and P. Lieberzeit, RSC Adv. **6**, 50414 (2016).
16) N. Palavesam, S. Marin, D. Hemmetzberger, C. Landesberger, K. Bock, and C. Kutter, Flex. Print. Electron. **3**, 014002 (2018).
17) M. Bosi and C. Pelosi, Prog. Photovoltaics. **15**, 51 (2006).
18) L. A. Coldren, IEEE J. Lightwave Technol. **29**, 554 (2011).
19) J. K. Doylend and A. P. Knights, Laser Photon. Rev. **6**, 504 (2012).
20) R. Nagarajan et al., Semicond. Sci. Technol. **27**, 094003 (2012).
21) P. P. Absil, P. Verheyen, P. De Heyn, M. Pantouvaki, G. Lepage, J. De Coster, and J. Van Campenhout, Opt. Express **23**, 9369 (2015).
22) W. Zhou, Z. Ma, H. Yang, Z. Qiang, G. Qin, H. Pang, L. Chen, W. Yang, S. Chuwongin, and D. Zhao, Appl. Phys. **42**, 234007 (2009).
23) L. Li, H. Lin, S. Qiao, Y. Zou, S. Danto, K. Richardson, J. D. Musgraves, N. Lu, and J. Hu, Nature Photon. **8**, 643 (2014).
24) T. Amemiya, T. Kanazawa, T. Hiratani, D. Inoue, Z. Gu, S. Yamasaki, T. Urakami, and S. Arai, Opt. Express **25**, 18537 (2017).
25) G. Ogawa, N. Sugiyama, M. Kanda, and K. Okano, Reports Res. Lab. Asahi Glass Co., Ltd. **55**, 47 (2005).
26) A. Campo and C. Greiner, J. Micromech. Microeng. **17**, R81 (2007).
27) V. Dolores-Calzadilla, D. Heiss, and M. Smit, Opt. Lett. **39**, 2786 (2014).
28) J. Kang, Y. Atsumi, Y. Hayashi, J. Suzuki, Y. Kuno, T. Amemiya, N. Nishiyama, and S. Arai, IEEE Journal of Sel. Top. Quantum Electron. **20**, 8202308 (2014).
29) Y. Kuno, J. Kang, Y. Hayashi, J. Suzuki, T. Amemiya, N. Nishiyama, and S. Arai, Jpn. J. Appl. Phys. **54**, 04DG04 (2015).